Improved optical coupling based on a concave cavity lens fabricated by optical fiber facet etching

Kanglin Li (李康林), Jiangbing Du (杜江兵)[*], Weihong Shen (沈微宏), Jiacheng Liu (刘嘉程), and Zuyuan He (何祖源)[**]

State Key Laboratory of Advanced Optical Communication Systems and Networks, Shanghai Jiao Tong University, Shanghai 200240, China

[*]Corresponding author: dujiangbing@sjtu.edu.cn
[**]Corresponding author: zuyuanhe@sjtu.edu.cn

We report a low-fabrication-complexity and wideband fiber lens, which is formed by fiber facet etching and filling high refractive index UV adhesive. The optical field can be significantly shrunk by the facet lens so as to obtain improved optical coupling. Numerical simulations were carried out for different coupling conditions, on both fundamental mode and high-order mode, for a nine-mode fiber. The fundamental mode area can be reduced from 152.17 to 12.57 μm^2, and the coupling loss between the fiber lens and a photonic waveguide can be reduced to -2.9 dB with over 1000 nm 3 dB bandwidth.

Keywords: fiber lens; optical coupling.
DOI: 10.3788/COL202119.050602

1. Introduction

With the continuously increasing demand of Internet services and applications, the bandwidth of the optical fiber communication network increases by 30%–50% every year[1–3]. Especially with the development of integrated photonics, optical coupling between optical fibers and integrated waveguides in photonic integrated circuits (PICs) has attracted more and more attention[4–12]. Edge coupling, vertical coupling, and adiabatic coupling are three major kinds of coupling methods from the optical fiber to the PIC. Although edge coupling provides broadband and polarization-insensitive optical coupling properties, it requires high coupling accuracy[13–15]. Vertical coupling is mostly in the form of grating coupling, and, compared to edge coupling, vertical coupling can reduce the alignment tolerance and simplify the measurement and packaging process[16]. Adiabatic coupling can achieve high efficiency, broadband, and a compact coupling area through the instantaneous power transmission of the waveguide taper[17,18].

In order to improve the coupling efficiency between the fiber and the PIC, the fiber lens is widely used[19,20]. But, traditional optical fiber lenses realized by the fusion method[21], fused taper method[22], and grinding and polishing method[23,24], are usually complicated, costly, and not suitable for mass production. In addition, the high-efficiency optical fiber lens can also be made by focused ion beam (FIB) etching[25–27].

In this work, we propose a low-fabrication-complexity concave cavity lens fabricated by optical fiber facet etching, the so-called facet etched cavity lens (FECL). The FECL is designed for shrinking the optical field area output from the fiber so as to improve optical coupling between the fiber and PICs. The fabrication principle of FECL is based on the graded index of the fiber showing different etching rates. Here, we chose the graded-index nine-mode fiber (NMF) to fabricate the FECL. We demonstrated the single-mode coupling between the fiber and on-chip waveguide [TE0-linearly polarized (LP01)] for supporting standard applications and high-order mode coupling (TE1-LP11) for supporting mode division multiplexing (MDM) applications.

Numerical simulation results show that the effective spot area of the fundamental mode (LP01) output from the FECL can be reduced from 152.17 to 12.57 μm^2, and the effective area of the LP11 mode can be reduced from 276.91 to 27.15 μm^2. The coupling loss of the fundamental mode between the FECL and on-chip inverse taper is reduced to 2.9 dB, and the coupling loss of the LP11 mode to the integrated Y-junction waveguide is down to 0.55 dB. The longitudinal tolerance for 80% coupling efficiency exceeds 20 μm.

2. Principle and Design

The FECL can be only formed on the fiber facet with the graded index decreasing from the center to around. Thus, we used an NMF to make the experimental demonstration, for instance. The fabrication process of the FECL is also applicable for other graded-index fibers, and the light focusing effect is the same. Figure 1 shows the schematic diagram of the proposed FECL for light focusing. The optical beam from the fiber before etching has a certain divergence angle, which is related to the numerical
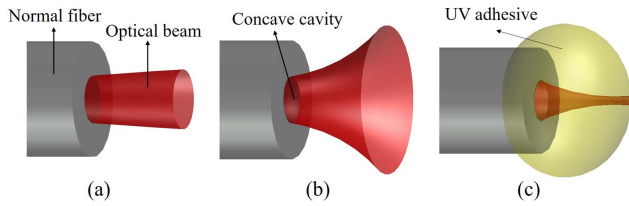
Fig. 1. Schematic diagram of the output optical beam from (a) a normal fiber facet, (b) the fiber facet with concave cavity, and (c) the FECL with UV adhesive.

Fig. 2. Schematic of the FECL fabrication process.

aperture (NA) of the fiber, as shown in Fig. 1(a). When coupling from the fiber to integrated waveguides, large coupling loss will be induced due to the large optical field mismatch as well as the divergence angle. After facet etching to form the concave cavity, the optical beam would be enlarged due to the increased divergence angle induced by the cavity, as shown in Fig. 1(b). However, after filling the concave cavity with high-index UV adhesive, the concave cavity becomes a convex lens, the so-called FECL, as shown in Fig. 1(c). Consequently, the optical beam is shrunk by the FECL. Simultaneous optical packaging can be realized after UV curing to solidify the adhesive. The focusing effect as well as the optical packaging performance of the FECL is highly dependent on the facet cavity structure and adhesive index.

Chemical etching is a very simple and low-cost method to fabricate the facet concave cavity. The principle of the fabrication is based on the different etching speeds between the core and the cladding. For standard fibers with germanium-doped cores and pure silica cladding, the core has a faster etching speed than the cladding in HF acid solution[28]. Theoretical analysis and experimental results show that the shape of the regular concave microcavity at the fiber core is determined by the reaction time, temperature, solution concentration, and so on[28–30]. The bond energy between the germanium atom and oxygen atom in germanium dioxide is 622 kJ/mol, and the bond energy between the silicon atom and oxygen atom in silicon dioxide is 799 kJ/mol[28], which means that germanium dioxide is more likely to react with the HF acid. With higher concentration of germanium in the fiber core, there will be a deeper reaction depth in the core than that in the cladding under the same conditions.

Figure 2 shows the fabrication process for the FECL with several steps: (a) fiber facet etching by simply putting the fiber end into the HF acid solution, with certain conditions of HF concentration, temperature, as well as etching duration; (b) fiber facet cleaning using alkaline water, alcohol, and clear water in turn; (c) drying up the fiber and forming the concave cavity on the fiber facet; (d) filling up the cavity and the gap between the fiber facet and photonic device with UV adhesive; (e) UV curing for solidifying the adhesive; (f) optical packaging completed.

Shown in Fig. 3 are the measured microscope images and height distribution diagram of two kinds of fibers after the HF acid etching: graded-index NMF and graded-index optical multimode (OM4) fiber. As expected, the core and the cladding have different etching speeds; thus, cavities can be realized
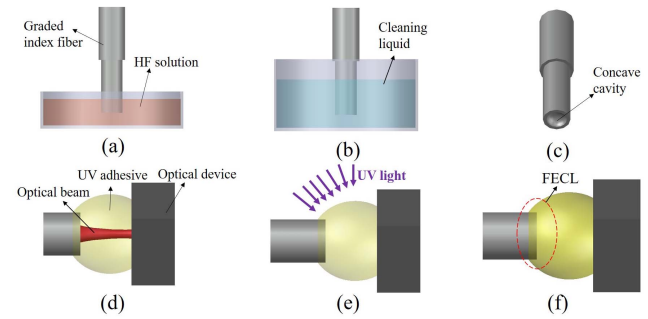
after a period of etching time. As for the graded-index fibers in Figs. 3(a) and 3(c), the facet microcavities are in paraboloid-like shape, so as to support the formation of the FECL. The sectional height distribution diagrams of the NMF and OM4 fiber measured by optical three-dimensional (3D) microscope are shown in Figs. 3(b) and 3(d), showing a clear concave cavity on the fiber facet.

We investigated the optical coupling of the FECL based on the NMF for both the fundamental mode and high-order mode for MDM applications. The NMF, as one kind of few-mode fiber, has a graded-index core profile with 33 µm core diameter and 125 µm cladding diameter. The core of this fiber is doped by germanium with the highest refractive index at the core center, and the cladding is pure silicon dioxide. Thus, the refractive index reaches the peak at the core center, and gradually decreases from the center. Such distribution of the refractive index is necessary to form the FECL after HF etching.

We carried out the experiment of NMF facet etching with different etching time. Shown in Fig. 4 is the cavity depth curve as a
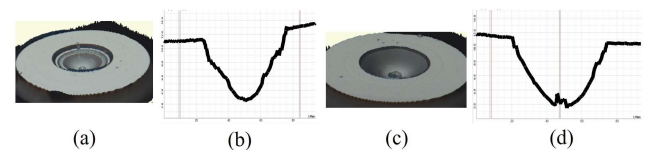

Fig. 3. Measured microscope images and sectional height profiles of the etched fiber facet: (a) NMF facet, (b) NMF height profile, (c) OM4 multimode fiber facet, (d) OM4 multimode fiber height profile.
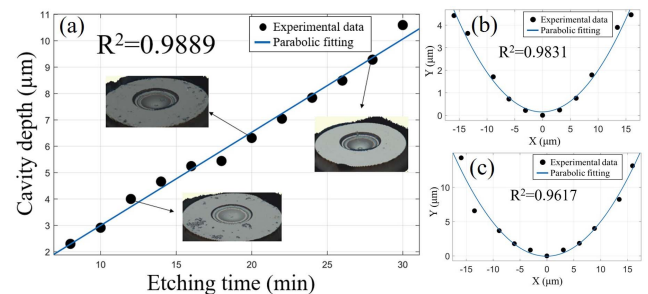

Fig. 4. (a) Measured cavity depths of NMF under etching time varying from 8 to 30 min. (b) and (c) are height profiles with paraboloid fitting after 12 min and 28 min etching, respectively.

function of etching time with 50% HF concentration acid under room temperature of 25°C. The linear fitting coefficient of the curve is $R^2 = 0.9889$, indicating that the cavity depth is proportional to the etching time, which is in good agreement with previous works[28,29].

We measured the profile of the facet cavity by using a high-resolution 3D microscope, as shown in Fig. 4. The height profiles of the cavities are shown in Figs. 4(b) and 4(c) after 12 min and 28 min etching, respectively. Paraboloid fitting, with a function of $Z = K(X^2 + Y^2)$, is used for characterizing the cavities with fitting accuracy of 0.1 μm. K represents the parabolic coefficient, which is related to the curvature of the facet cavity and determined by the etching time. The fitting coefficients R^2 of Figs. 4(b) and 4(c) are 0.9831 and 0.9617, respectively.

Another important factor determining the FECL performance is the refractive index of the UV adhesive (N_{UV}). Generally, when using UV adhesive with a higher refractive index, better focusing performance of the FECL can be realized. The UV adhesive with the highest refractive index available in the market is about 1.65. Thus, we use the adhesive refractive index around 1.6 for further investigations. We carried out simulations for the FECL to verify the optical focusing effect, for both fundamental mode and high-order mode. The simulation is adopted by the 3D finite-difference time-domain (FDTD) method.

3. FECL for Optical Focusing

Figure 5 shows the output optical fields of the fundamental mode from the NMF facet in three different cases, without etching, with facet etched concave cavity ($K = 0.12$), and FECL after high-index UV adhesive ($N_{UV} = 1.6$) filling, respectively. One can clearly observe the optical focusing effect after the FECL due to the formation of a convex lens on the fiber facet. Under different FECL structures (i.e., different shape coefficient K and index N_{UV} of the facet lens), we can obtain different optical focusing performance for various optical coupling applications.

The output optical beams of the fundamental mode after different FECLs are shown in Figs. 6(a)–6(d), with K ranging from 0.09 to 0.15 at a step of 0.02, while N_{UV} is fixed to 1.6, and the optical wavelength is fixed at 1550 nm. Steady enhancement of

Fig. 6. Simulated fundamental mode optical beams: (a) $K = 0.09$, (b) $K = 0.11$, (c) $K = 0.13$, (d) $K = 0.15$ with fixed N_{UV} value at 1.6; (e) $N_{UV} = 1.56$, (f) $N_{UV} = 1.6$, (g) $N_{UV} = 1.64$, (h) $N_{UV} = 1.68$ with fixed K value at 0.12.

optical focusing can be observed clearly. Then, we fix K at 0.12 and hold the optical wavelength at 1550 nm, and the output optical beams are shown in Figs. 6(e)–6(f) after FECL with N_{UV} ranging from 1.56 to 1.68 at a step of 0.04. Improved optical focusing can also be observed along with the increased adhesive index, which is in good agreement with our above-mentioned predictions.

Here, we define the effective area reduction ratio to estimate the performance of optical beam focusing, which is calculated by the ratio of the effective field area between the original fundamental mode and the waist after FECL. Figure 7 shows the to K and N_{UV}. In the NMF, the original effective area of the fundamental mode is as large as 152.17 μm^2, as shown in the inset figure of Fig. 7(1). Figures 7(2)–7(5) present the optical field of the fundamental mode after FECL at the focus plane, which has the minimum optical field. With typical value of 1.64 for the UV adhesive index and 0.14 for K, a shrunken area of only 12.57 μm^2 is obtained.

The focusing performance of FECL is also affected by the longitudinal offset, as shown in Fig. 8, in which the spot effective area varies along with different longitudinal displacements. The reference position is 12 μm from the FECL, with K changing
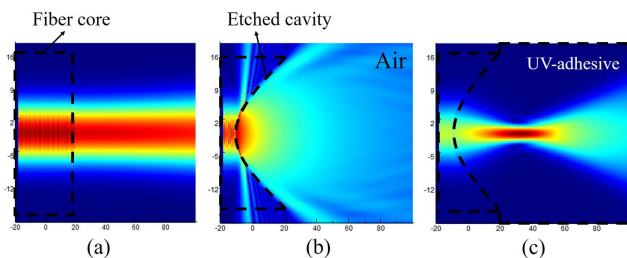

Fig. 5. Simulated optical beam field of the output fundamental mode: (a) NMF without etching, (b) facet cavity without filling the UV adhesive, and (c) FECL with UV adhesive.
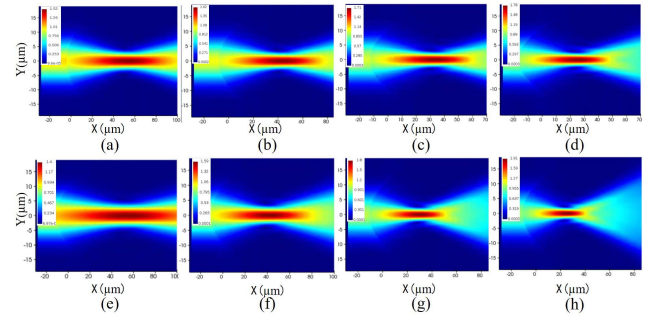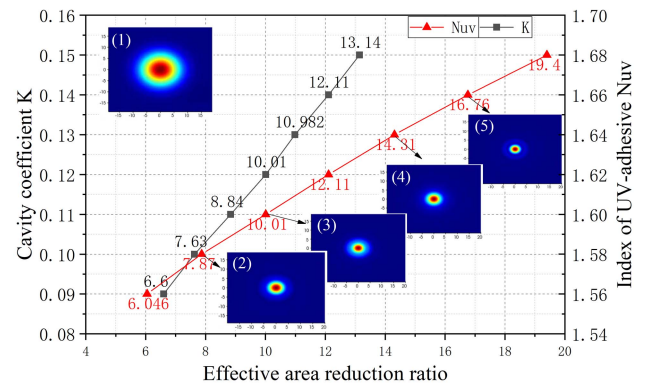

Fig. 7. Simulated reduction of the effective area of fundamental mode. The inset figures: (1) fundamental mode in the NMF; (2)–(5) shrunken mode fields of different FECLs.
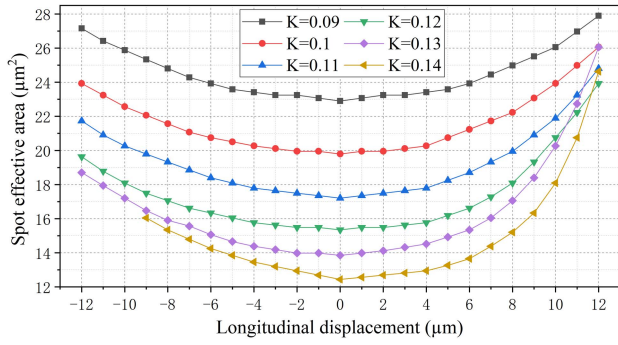
Fig. 8. Simulated longitudinal displacement tolerance of fundamental mode spot effective area at different K.

from 0.09 to 0.14 and N_{UV} fixed at 1.6, so as to reach the beam waist.

The focusing performance of higher-order mode LP11 after FECL is also investigated, as shown in Fig. 9. The propagated optical beams are shown in Figs. 9(a)–9(d), with K changing from 0.09 to 0.15 at a step of 0.02, and N_{UV} fixed at 1.6 at a wavelength of 1550 nm. The K value is fixed at 0.12, and the N_{UV} is changed from 1.56 to 1.68 at a step of 0.04, as shown in Fig. 9(e)–9(h).

We calculated the LP11 mode effective area at the waist after different FECLs. Shown in Fig. 10 is the effective area reduction ratio as a function of K and N_{UV}. The original optical effective area of the LP11 mode is as large as 276.91 μm^2, as shown in Fig. 10(1). The optical field of the LP11 mode after the FECL at the focus plane of the FECL has the minimum optical field, as shown in the inset figures of Fig. 10(2)–10(5). A shrunken area of 27.15 μm^2 can be obtained, with value of 1.64 for the UV adhesive index and 0.14 for K. The tolerance of the longitudinal offset of the spot effective area is shown in Fig. 11, with K changing from 0.09 to 0.14, and N_{UV} fixed at 1.6.

In this work, we mainly investigate the performance of FECL by simulating the coupling loss of FECL to photonic chips. An inverse taper can be used for on-chip transmission of the fundamental mode; but, for high-order modes, we need specially
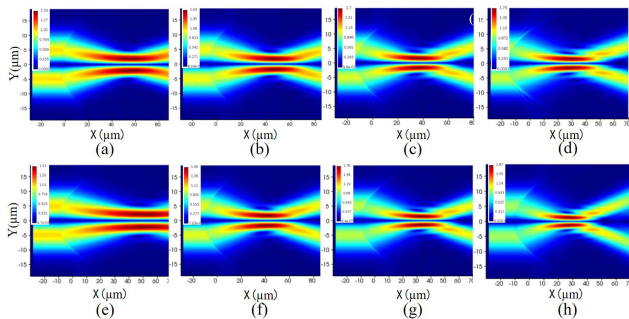

Fig. 9. Simulated LP11 mode optical field simulation: (a) $K = 0.09$, (b) $K = 0.11$, (c) $K = 0.13$, (d) $K = 0.15$, (e) N_{UV}=1.56, (f) $N_{UV} = 1.6$, (g) $N_{UV} = 1.64$, and (h) $N_{UV} = 1.68$. The N_{UV} value is fixed at 1.6 in (a)–(d) and the K value at 0.12 in (e)–(h), respectively.
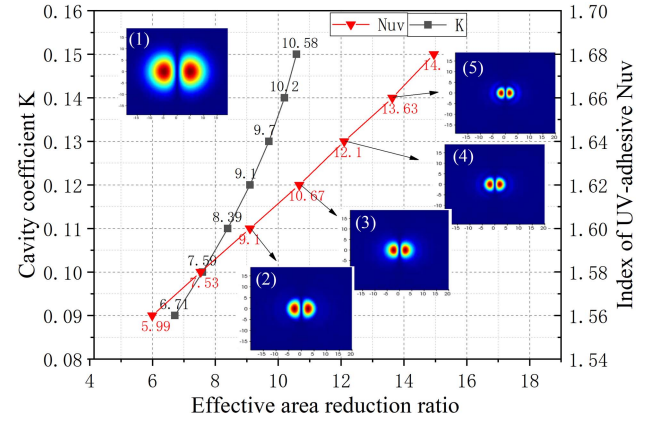

Fig. 10. Simulated reduction of the effective area of the LP11 mode. The inset figures: (1) LP11 mode in the NMF; (2)–(5) shrunken mode fields after different FECLs.
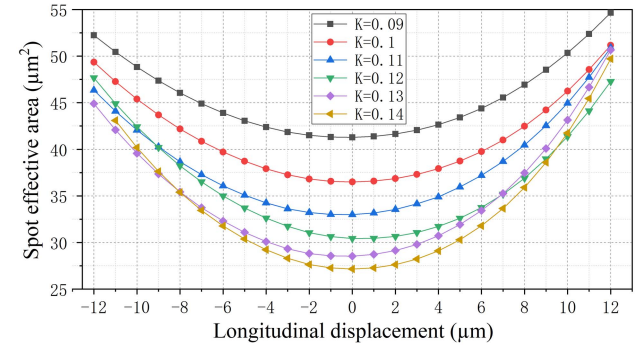

Fig. 11. Simulated longitudinal displacement tolerance of the LP11 mode spot effective area after different FECLs. Displacement from the minimum spot area from plus to minus 12 μm.

shaped waveguides like the Y-junction inverse taper. The schematic diagrams of these waveguides are shown in Fig. 12. The dimension of the inverse taper is fixed, as shown in Fig. 12(a). The widths of the waveguide tip W_1 and main waveguide W_2 are 150 nm and 450 nm, respectively. The height of the waveguide H_1, is 220 nm as shown in Fig. 12(b). Figure 12(c) is the schematic diagram of the Y-junction inverse taper waveguide, in which two separated inverse tapers are combined into one main waveguide. Three structural parameters including the width of the taper tip (W_3), the width of the main waveguide (W_4), and the distance between the two inverse tapers (W_S) can be optimized.

The coupling efficiencies of edge coupling from the FECL to inverse tapers are calculated for characterizing the coupling functionality of the FECL. Figure 13 shows the fundamental mode longitudinal and lateral coupling loss tolerance from the FECL to the inverse taper, under different K values and a fixed value of N_{UV} at 1.6. Generally, the better the matching between the focused mode field of the FECL and the inverse taper, the higher the coupling efficiency realized. It can be found
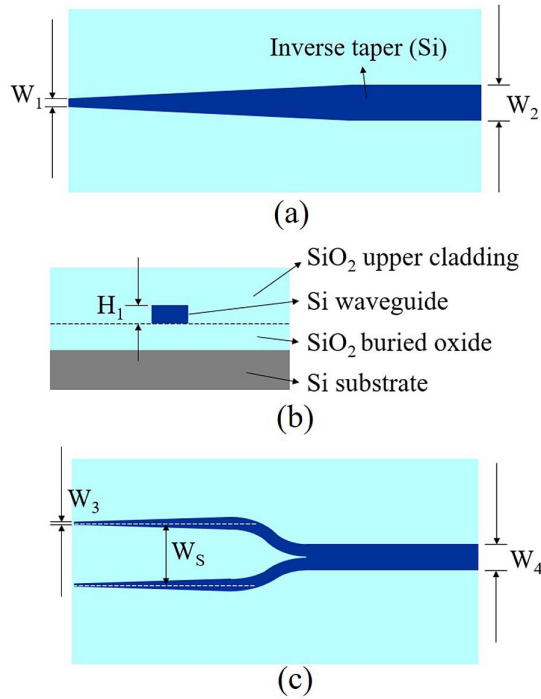
Fig. 12. Schematic diagram of two kinds of inverse tapers: (a), (b) the top view and sectional view of the inverse taper and (c) top view of the Y-junction inverse taper waveguide.

that higher K value leads to higher optimal coupling efficiency, but with lower coupling tolerance, as shown in Fig. 13.

Table 1 shows the optimal coupling distance and 80% coupling tolerance of fundamental mode coupling from the NMF FECL to the inverse taper. The coupling distance (about 20 μm) and tolerance in the longitudinal direction (mainly over 30 μm) of the proposed FECL are both larger than those of the conventional fiber lens. Besides, the use of FECL can also simplify the packaging, leading to reduced packaging cost and higher yield.

The high-order mode (LP11) edge coupling needs a special shape of waveguide like the Y-junction inverse taper waveguide, as shown in Fig. 12(c). The two separated inverse tapers can be well coupled with the two speckles of the LP11 mode. Besides K and N_{UV}, the distance between the two inverse tapers (W_S) also
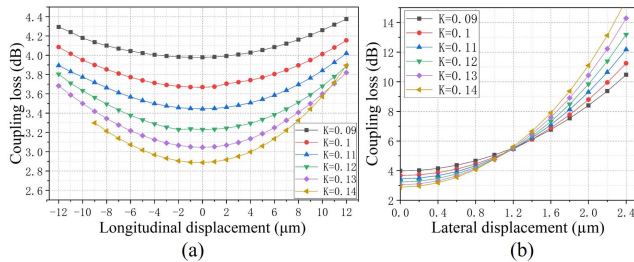

Fig. 13. Simulated coupling efficiency of the fundamental mode from the FECL to the inverse taper under different cavity coefficient K: (a) longitudinal coupling tolerance along with longitudinal displacement and (b) lateral coupling tolerance along with horizontal alignment.

Table 1. Simulated Optimal Coupling Distance, Longitudinal and Lateral 80% Coupling Tolerance of Fundamental Mode Coupling from Fiber to Inverse Taper.

K	0.09	0.10	0.11	0.12	0.13	0.14
Optimal coupling distance (μm)	34	28	23	17	13	9
80% longitudinal tolerance (μm)	> 40	> 40	> 30	> 30	29	20
80% lateral tolerance (μm)	2.0	1.8	1.6	1.6	1.5	1.4

deeply affects the coupling efficiency. With the improvement of the optical focusing effect, the value of W_S needs to be reduced for more accurate coupling. Figure 14 shows the longitudinal and lateral tolerance for LP11 coupling from the fiber to the Y-junction waveguide. The coupling loss firstly increases along with the lateral displacement, and then a small reduction is observed, which is due to the leaking of the optical field when the lateral displacement is too large, as shown in Fig. 14(b). The 80% coupling loss and optimal W_S are shown in Table 2, and the optimal coupling distance of the LP11 mode is almost the same as the fundamental mode.

The wideband transmission of the fundamental mode and high-order mode coupling is also investigated as shown in Fig. 15. For the fundamental mode in Fig. 15(a), the 3 dB bandwidth is over 1000 nm. For the high-order mode LP11 in Fig. 15(b), the 3 dB bandwidth is smaller, but still over 900 nm.

The reason why we have not carried out the coupling experiment was limited by objective factors; according to our
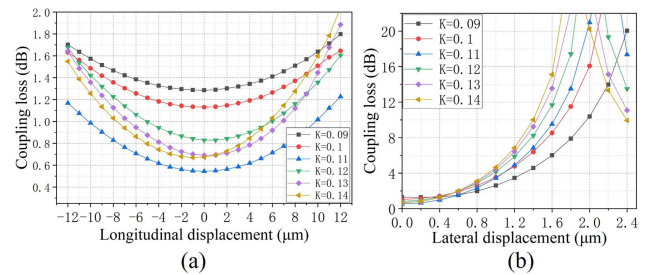

Fig. 14. Simulated coupling efficiency of the LP11 mode coupling from the fiber to the Y-junction inverse taper with different K: (a) coupling tolerance at the optimal coupling point in the longitudinal direction and (b) lateral coupling tolerance of the coupling efficiency.

Table 2. Simulated Optimal W_S Value, Longitudinal and Lateral Coupling Tolerance with 80% Efficiency, for LP11 Coupling from Fiber to Y-Junction Inverse Tapers.

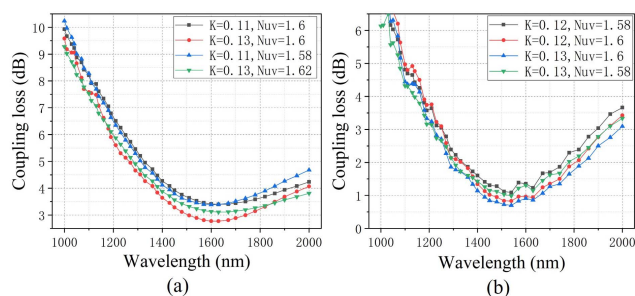| K	0.09	0.10	0.11	0.12	0.13	0.14
W_S (μm)	4.1	4.0	3.7	3.6	3.4	3.4
80% longitudinal tolerance (μm)	> 40	> 40	> 30	> 30	29	20
80% lateral tolerance (μm)	2.0	1.8	1.6	1.6	1.5	1.4

Fig. 15. Simulated transmission spectrum of the FECL coupling to inverse taper for (a) the fundamental mode and (b) the LP11 mode.

simulation, in order to achieve high coupling efficiency from the FECL to the optical waveguide, the parabolic coefficient K, which is related to the curvature of the facet cavity, must reach about 0.13, where the corresponding corrosion depth is about 35 μm. However, although we found the linear relationship between etching depth and time, limited by our experimental conditions, the shape and depth of the microcavity formed by HF acid corrosion for a long time are not ideal. But, the desired experimental results have been realized in other's work[26], which proved that this fabrication method is practicable and reliable.

4. Conclusion

As a conclusion, in this work, we propose a new kind of fiber lens named FECL for optical coupling with low-fabrication-complexity and wideband operation. The FECL is fabricated by fiber facet etching and filling the high refractive index UV adhesive in the etched concave cavity. The simulation results show that, at the wavelength of 1550 nm, the fundamental mode spot area of the NMF can be reduced from 152.17 to $12.57\,\mu m^2$, and the effective area of the LP11 mode can be reduced from 276.91 to $27.15\,\mu m^2$. The edge coupling loss from the NMF to the integrated waveguide is 2.9 dB with over 1000 nm 3 dB bandwidth, and the coupling loss of the LP11 mode to the Y-junction waveguide is reduced to 0.55 dB with over 900 nm 3 dB bandwidth. In addition to optical coupling between fibers and photonic waveguides, the proposed FECL also has great potential for other optical coupling and packaging applications.

Acknowledgement

References

1. S. Jiang, L. Ma, S. Wang, X. Fan, and Z. He, "Mode-interference-induced oscillation in propagation speed of fiber fuse in few-mode fibers," Opt. Lett. **43**, 4252 (2018).

2. W. Shen, J. Du, L. Sun, C. Wang, Y. Zhu, K. Xu, B. Chen, and Z. He, "Low-latency and high-speed hollow-core fiber optical interconnection at 2-micron waveband," J. Lightwave Technol. **38**, 3874 (2020).

3. R. Essiambre, G. Kramer, P. J. Winzer, G. J. Foschini, and B. Goebel, "Capacity limits of optical fiber networks," J. Lightwave Technol. **28**, 662 (2010).

4. L. Ma, S. Jiang, J. Du, C. Yang, W. Tong, and Z. He, "Ring-assisted 7-lp-mode fiber with ultralow inter mode crosstalk," in *Asia Communications and Photonics Conference 2016* (Optical Society of America, 2016), paper AS4A.5.

5. Y. Liu, L. Ma, W. Xiao, R. Wang, J. Xiong, J. Luo, and Z. He, "Wide band multimode fiber with an optimized core size and fluorine-doped cladding for high-speed SWDM and CWDM transmission," Opt. Express **27**, 15433 (2019).

6. S. Jiang, L. Ma, Z. Zhang, X. Xu, S. Wang, J. Du, C. Yang, W. Tong, and Z. He, "Design and characterization of ring-assisted few-mode fibers for weakly coupled mode-division multiplexing transmission," J. Lightwave Technol. **36**, 5547 (2018).

7. J. Li, J. Du, L. Ma, M.-J. Li, and Z. He, "Second-order few mode distributed Raman amplifier for mode-division multiplexing transmission," in *Optical Fiber Communication Conference* (Optical Society of America, 2017), paper Th4A.3.

8. G. Son, S. Han, J. Park, K. Kwon, and K. Yu, "High-efficiency broadband light coupling between optical fibers and photonic integrated circuits," Nanophotonics **10**, 1515 (2018).

9. J. Li, C. Cai, J. Du, S. Jiang, L. Ma, L. Wang, L. Zhu, A. Wang, M. Li, H. Chen, J. Wang, and Z. He, "Ultra-low-noise mode-division multiplexed WDM transmission over 100-km FMF based on a second-order few-mode Raman amplifier," J. Lightwave Technol. **36**, 3254 (2018).

10. L. Jia, C. Li, T.-Y. Liow, and G.-Q. Lo, "Efficient suspended coupler with loss less than −1.4 dB between Si-photonic waveguide and cleaved single mode fiber," J. Lightwave Technol. **36**, 239 (2018).

11. R. Marchetti, C. Lacava, L. Carroll, K. Gradkowski, and P. Minzioni, "Coupling strategies for silicon photonics integrated chips," Photon. Res. **7**, 201 (2019).

12. D. Vermeulen, S. Selvaraja, P. Verheyen, G. Lepage, W. Bogaerts, P. Absil, D. V. Thourhout, and G. Roelkens, "High-efficiency fiber-to-chip grating couplers realized using an advanced CMOS-compatible silicon-on-insulator platform," Opt. Express **18**, 18278 (2010).

13. T. Shoji, T. Tsuchizawa, T. Watanabe, K. Yamada, and H. Morita, "Low loss mode size converter from 0.3 μm square Si wire waveguides to single mode fibres," Electron. Lett. **38**, 1669 (2002).

14. F. Van Laere, G. Roelkens, and M. Ayre, "Compact and highly efficient grating couplers between optical fiber and nanophotonic waveguides," J. Lightwave Technol. **25**, 151 (2007).

15. H. Park, S. Kim, J. Park, J. Joo, and G. Kim, "A fiber-to-chip coupler based on Si/SiON cascaded tapers for Si photonic chips," Opt. Express **21**, 29313 (2013).

16. A. Bozzola, L. Carroll, D. Gerace, I. Cristiani, and L. C. Andreani, "Optimising apodized grating couplers in a pure SOI platform to −0.5 dB coupling efficiency," Opt. Express **23**, 16289 (2015).

17. T. G. Tiecke, K. P. Nayak, J. D. Thompson, T. Peyronel, N. P. de Leon, V. Vuletić, and M. D. Lukin, "Efficient fiber-optical interface for nanophotonic devices," Optica **2**, 70 (2015).

18. A. Khilo, M. A. Popović, M. Araghchini, and F. X. Kärtner, "Efficient planar fiber-to-chip coupler based on two-stage adiabatic evolution," Opt. Express **18**, 15790 (2010).

19. P. Li, J. Liu, P. Huang, X. Zhang, J. Shi, L. Yuan, and C. Guan, "Tunable fiber-tip lens based on thermo-optic effect of amorphous silicon," Chin. Opt. Lett. **18**, 030602 (2020).

20. X. Zhang, T. Yuan, X. Yang, C. Guan, J. Yang, Z. Liu, H. Deng, and L. Yuan, "In-fiber integrated optics: an emerging photonics integration technology [Invited]," Chin. Opt. Lett. **16**, 110601 (2018).

21. J. I. Yamada, Y. Murakami, and J. I. Sakai, "Characteristic of a hemispherical microlens for coupling between a semiconductor laser and single mode fiber," IEEE J. Quantum Electron **16**, 1067 (1980).

22. F. P. Payne, C. D. Hussey, and M. S. Hataki, "Modelling fused single-mode fibre couplers," Electron. Lett. **21**, 461 (1985).

23. S.-M. Tseng and C.-L. Chen, "Side-polished fibers," Appl. Opt. **31**, 3438 (1992).

24. V. K. S. Hsiao, Z. Li, Z. Chen, P. C. Peng, and J. Tang, "Optically controllable side-polished fiber attenuator with photo responsive liquid crystal over lay," Opt. Express **17**, 19988 (2009).

25. H. Melkonyan, K. Sloyan, M. Odeh, and I. Almansouri, "Embedded parabolic fiber lens for efficient fiber-to-waveguide coupling fabricated by focused ion beam," J. Phys. Photon. **1**, 025004 (2019).

26. H. Melkonyan, K. Sloyan, K. Twayana, P. Moreira, and M. Dahlem, "Efficient fiber-to-waveguide edge coupling using an optical fiber axicon lens fabricated by focused ion beam," IEEE Photon. J. **9**, 7104309 (2017).

27. H. Melkonyan, K. Sloyan, M. Odeh, and I. Almansouri, "Gradient-index optical fiber lens for efficient fiber-to-chip coupling," Opt. Express **25**, 13035 (2017).

28. P. A. R. Tafulo, P. A. S. Jorge, J. L. Santos, and O. Frazão, "Fabry–Pérot cavities based on chemical etching for high temperature and strain sensing," Opt. Commun. **285**, 1159 (2012).

29. C. J. Tuck, R. Hague, and C. Doyle, "Low cost optical fibre based Fabry–Perot strain sensor production," Meas. Sci. Technol. **17**, 2206 (2006).

30. Y. Gong, Y. J. Rao, Y. Guo, Z. L. Ran, and Y. Wu, "Temperature insensitive micro Fabry–Pérot strain sensor fabricated by chemically etching Er-doped fiber," IEEE Photon. Technol. Lett. **21**, 1725 (2009).